IONIZATION AND EXCITATION IN COOL GIANT STARS. I. HYDROGEN AND HELIUM

Donald G. Luttermoser[1]

Joint Institute for Laboratory Astrophysics, University of Colorado and National Institute for Standards and Technology,
Boulder, CO 80309-0440

AND

Hollis R. Johnson

Astronomy Department Indiana University, Bloomington, IN 47405

ABSTRACT

We demonstrate the influence that non–LTE radiative transfer has on the electron density, ionization equilibrium, and excitation equilibrium, in model atmospheres representative of both oxygen-rich and carbon-rich red giant stars. The radiative transfer and statistical equilbrium equations are solved self-consistently for H, H^-, H_2, He I, C I, C II, Na I, Mg I, Mg II, Ca I, and Ca II in a plane-parallel static medium. Calculations are made for both (a) radiative-equilibrium model photospheres alone and (b) model photospheres with attached chromospheric models as determined semiempirically with IUE spectra of g Her (M6 III) and TX Psc (C6, 2). This paper reports on the excitation and ionization results for hydrogen and helium. The second paper in this series will concern itself with results obtained for the neutral metals and their importance to the electron density and H^- opacity.

Although hydrogen is strongly overionized with respect to LTE throughout much of the atmosphere of the photospheric models, almost all the hydrogen is still in the ground state or associated in H_2, and the hydrogen contribution to the electron density is small. Thus this overionization has little impact on the atmospheric structure or the emergent spectrum. Similar, even stronger, results are found for helium. Radiative equilibrium models converged with polyatomic molecular opacities have hydrogen ionization and excitation equilibria that are fundamentally different than those models converged with diatomic molecular opacities alone. The Lyman lines control the ionization and excitation in these model atmospheres. Carbon abundance influences the ionization and excitation of hydrogen through the strong C I bound-free opacity under the Lyman lines—carbon stars are overionized and overexcited in hydrogen with respect to oxygen-rich stars of similar temperatures and surface gravities. Attaching a chromospheric temperature rise to the outer layers further increases the ionization in the upper photosphere from "chromospheric backwarming." Partial redistribution effects in Lyα have significant consequences in the ionization and excitation of hydrogen in the temperature minimum region of the g Her chromospheric-photospheric model and the lower chromosphere of the TX Psc model. Although the Lyman lines are very optically thick throughout much of these models, detailed balance does not hold for these lines, and detailed radiative transfer plays a fundamental role in the ionization and excitation of hydrogen throughout the entire atmospheres. Helium is ionized only slightly in these chromospheric models, and its ionization essentially plays no role.

Subject headings: radiative transfer — stars: atmospheres — stars: late-type

1. INTRODUCTION

Particle densities in the upper photospheres and chromospheres of late-type giant and supergiant stars are so low that atomic and molecular electronic transitions are dominated by radiative instead of collisional processes (e.g., see Auman & Woodrow 1975; Hartmann & Avrett 1984; Jordan 1986). Because of this complicating circumstance and a lack of good observational data for stars later than M0, little research on ionization and excitation has actually been carried out. Readers are referred to the original papers for observational details concerning ionization and excitation for chromospheric depths of these late-type stars (Judge 1986a, b; Johnson & Luttermoser 1987; Eaton & Johnson 1988). An excellent review of photospheric modeling, including discussions on non–LTE (NLTE) ionization and excitation can be found in Carbon (1979). Other general reviews are given by Johnson (1986) and Judge (1989).

Among the few early workers to investigate quantitatively NLTE effects in the ionization equilibrium of late-type giant stars were Auman & Woodrow (1975). They found the neutral metals Na, Mg, Al, K, and Ca to be overionized with respect to LTE in atmospheres with effective temperatures less than 3000 K. However, they assumed all radiative bound-bound transitions to be in detailed balance and used coarse approximations in their calculation of photoionizations and collisional transitions. A semiempirical investigation of the ionization equilibrium in late-type giants was made by Ramsey (1977), who generated LTE synthetic spectra of the Ca I line at 6572 Å and the Ca II line at 7323 Å from radiative equilibrium models representative of α Tau, α Ori, β And, α Cet, μ Gem, and β Peg. A comparison between the synthetic line profiles and the observed profiles indicated overionization with respect to LTE, with α Ori exhibiting a very large overionization relative to LTE. However, this analysis was criticized by Desikachary & Gray (1978), due to the omission of a convolution of rotation and macroturbulence in the synthetic line profiles; and Luck & Lambert (1982) further showed that the contin-

579

uum placement near these calcium lines is also difficult. A semiempirical determination of photospheric structure for a red giant is still lacking.

Although the detailed balance approximation for bound-bound transitions is very convenient, we here demonstrate that it cannot be used in any low-density environment for transitions with large oscillator strengths. We present radiative transfer and statistical equilibrium calculations made with the PANDORA radiative transfer code (Vernazza, Avrett, & Loeser 1973, hereafter VAL I; 1976, hereafter VAL II; 1981, hereafter VAL III). As models representative of the coolest non-Mira red giants, we use radiative equilibrium models with the parameters, in the notation (T_{eff}/log g/C-to-O), of 3200/0.0/ 0.58 (Brown et al. 1989) and 3000/0.0/1.05 (Johnson 1982) to represent the photospheres of the M6 III star g Her and the N-type carbon star TX Psc, respectively. Semiempirical chromospheric models of Luttermoser, Johnson, & Eaton (1992, hereafter called the LJE model) and of Luttermoser et al. (1989, hereafter called the LJAL model) are used to represent the chromospheric plus photospheric layers of g Her and TX Psc, respectively. In addition, we also perform NLTE calculations with a 3100/−0.5/1.03 model of TX Psc which included polyatomic molecular opacities in the radiative equilibrium calculations. Spectra from this "polyatomic" photospheric model fit the infrared spectrum of TX Psc better than the radiative equilibrium portion of the LJAL model (Jørgensen 1989), and it fits the visual and UV as well (Johnson, Luttermoser, & Faulkner 1988). In some sense, these polyatomic models supersede the models with diatomic molecular opacities only. We must retain these older models, however, for the LJAL chromospheric model—the only model for a carbon star presently available—is based on it. The polyatomic opacity photosphere with attached hypothetical chromospheres have recently been tested for their influence on molecular band intensities (Jørgensen & Johnson 1991) and both photospheric models with attached hypothetical chromospheres have been subjected to the constraint of mass loss at the observed rate (Johnson 1991). The photosphere/chromosphere models used in this study are displayed in Figures 1a and 1b. Only the lower

chromospheric regions of these models are constrained by the observations; the upper chromospheres are just smooth extrapolations of the temperature-density structure of the inner chromospheres. Johnson, Jørgensen, & Luttermoser (1991) and Luttermoser & Brown (1992) discuss the shortcomings in the LJAL model.

Detailed discussions of the NLTE synthetic spectra calculations of the chromospheric-photospheric models, along with comparisons to observed spectra, and the selection of such stellar parameters (i.e., T_{eff}, log g, and microturbulent velocities) can be found in the references cited. Section 2 describes the atomic models and rate parameters for hydrogen and helium. Section 3 describes in detail the excitation and ionization of hydrogen. Section 4 describes the helium calculations, where it is shown that excitation and ionization of helium is negligible throughout the entire photosphere and lower chromosphere of these models. The hydrogen and helium calculations, described separately, are structured into two subsections; the first discusses ionization and excitation in the "pure" photospheric models, and the second describes the effect that the chromospheric radiation field has on the level populations both in the chromosphere *and* photosphere. Section 5 contains a discussion on these results and various problems encountered in NLTE modeling of cool, low-density environments and concluding remarks. Discussion of the H⁻ opacity will be made in the second paper in this series (Luttermoser 1992, hereafter Paper II); which presents results of the ionization and excitation of the neutral metals, since they are the major contributors to the electron density throughout much of these atmospheres.

2. ATOMIC MODELS

Many of the atomic data used in these radiative transfer and statistical equilibrium equations have been published elsewhere. The data for hydrogen, with their original references cited, can be found in VAL III, and updates to the hydrogen collisional rates can be found in Chang, Avrett, & Loeser (1991). The references for the neutral helium data are reported by Avrett, Vernazza, & Linsky (1976). The following presents a
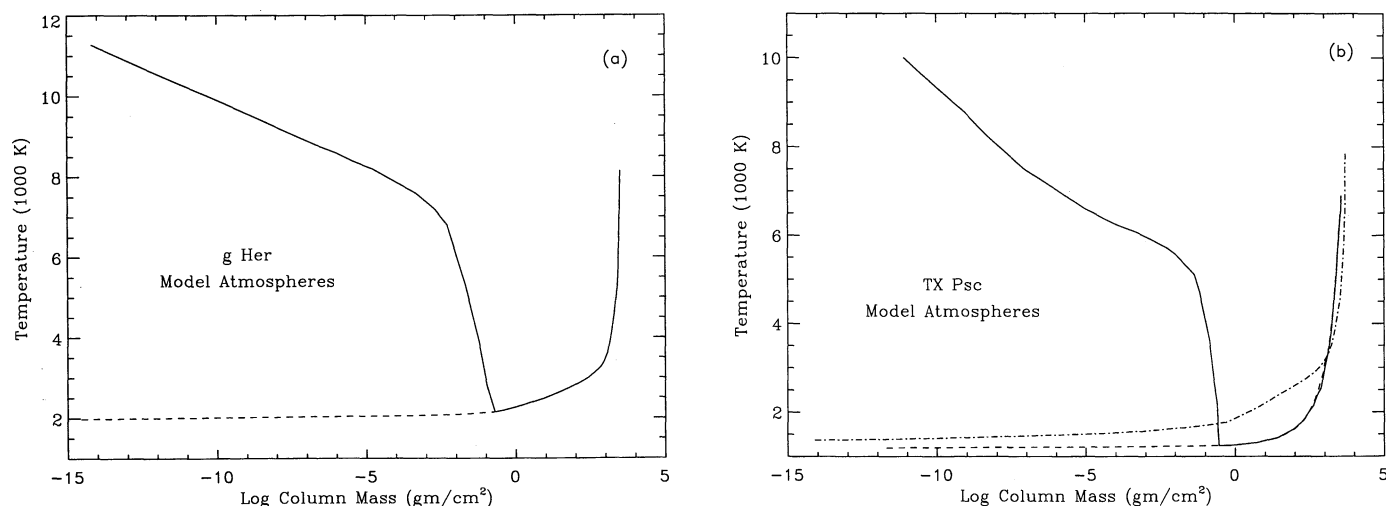

FIG. 1.—Thermal structure of several model atmospheres considered here. (a) Representative models of the M giant star g Her. The semiempirical chromospheric-photospheric (LJE) model is designated with a solid line and the "pure" photospheric model with a dashed line. (b) Various models representative of the N0 carbon star TX Psc. The semiempirical chromospheric-photospheric (LJAL) model is designated with a solid line, the photospheric models are designated with a dashed line for the Johnson (1982) model and a dot-dashed line for the Jørgensen (1989) model.

TABLE 1

PHOTOIONIZATION DATA FOR THE HYDROGEN ATOMIC MODEL

Level (i)	Notation	g_i	λ_i (Å)	σ_i (10^{-18} cm²)
1............	$1s\ ^2S$	2	911.76	7.906
2............	$2p\ ^2P^o$	8	3647.05	13.85
3............	$3p\ ^2P^o$	18	8205.87	21.58

summary of this data. We also reference publications for atomic data that has been updated from the VAL III and Avrett, Vernazza, & Linsky papers.

2.1. *Hydrogen*

We use a three-level hydrogen atom in the radiative transfer and statistical equilibrium calculations for the model atmospheres. Luttermoser et al. (1989) has shown that a three-level model for hydrogen is sufficient in these cool stellar environments for describing accurately both the emergent Balmer-α line profile and the contribution of hydrogen to the electron density. Our three-level model consists of the three lowest energy levels of the hydrogen atom. The spectroscopic notations, statistical weights, bound-free edge locations, and photoionization cross sections for the levels are listed in Table 1, and collisional ionization coefficients are included in Table 2. Rate equations for photoionization, radiative recombination, collisional ionization (which defines the collisional ionization coefficient), and collisional recombination are presented in the next section. There are three bound-bound transitions included in the atomic model: 2–1 (Lyα), 3–1 (Lyβ), and 3–2 (Hα). Table 2 also lists the collisional excitation coefficients for a grid of temperatures, where a linear interpolation is used to determine the coefficients at temperatures between the values given in the table, and linear extrapolating are used for temperatures above and below the maximum and minimum table temperatures.

Table 3 lists the Einstein A-values and line-broadening parameters for our three hydrogen transitions. The line-broadening half-widths of Table 3 are defined as follows: $C_{\rm rad}$ represents natural broadening, $C_{\rm vdW}$ is van der Waals broadening, $C_{\rm Stark}$ represents linear Stark broadening by electron collisions, and $C_{\rm res}$ is resonance broadening. The absorption coefficient for each line is assumed to have the frequency dependence of a Voigt profile $H(a, v)$, where $a = \delta/\Delta\lambda_{\rm D}$, v is the wavelength displacement from line center in Doppler units, and $\Delta\lambda_{\rm D}$ is the Doppler half-width. The line-broadening half-

TABLE 2

COLLISIONAL RATE COEFFICIENTS FOR THE HYDROGEN ATOMIC MODEL[a]

A. IONIZATION: $\Omega_i(T)$ (cm³ s⁻¹)

Level (i)	5000 K	9000 K	15,000 K	25,000 K	35,000 K
1...........	2.82(−9)	3.92(−9)	5.30(−9)	7.27(−9)	9.01(−9)
2...........	5.90(−8)	7.59(−8)	9.44(−8)	1.17(−7)	1.34(−7)
3...........	2.87(−7)	3.61(−7)	4.40(−7)	5.23(−7)	5.72(−7)

B. EXCITATION: $\Omega_{ji}(T)$ (cm³ s⁻¹)

Transition	5000 K	9000 K	15,000 K	25,000 K	35,000 K
2–1........	2.19(−8)	2.18(−8)	2.11(−8)	2.04(−8)	2.02(−8)
3–1........	7.62(−9)	6.63(−9)	6.30(−9)	6.61(−9)	7.29(−9)
3–2........	5.40(−7)	6.66(−7)	8.46(−7)	8.21(−7)	8.56(−7)

[a] Format $a\ .\ bc(y)$ corresponds to $a\ .\ bc \times 10^y$.

TABLE 3

EINSTEIN A-VALUES AND LINE BROADENING HALF-WIDTHS FOR THE HYDROGEN ATOMIC MODEL

Transition	$\lambda_{\rm vac}$ (Å)	A (10^8 s⁻¹)	$C_{\rm rad}$ (10^{-6} Å)	$C_{\rm vdW}$ (10^{-6} Å)	$C_{\rm Stark}$ (10^{-6} Å)	$C_{\rm res}$ (10^{-6} Å)
2–1.......	1215.669	4.699	18.4	9.11	0.02	26.6
3–1.......	1025.721	0.5575	2.785	11.5	0.03	3.00
3–2.......	6564.607	0.441	650.	440.	1174.	898.

width δ is given by

$$\delta = C_{\rm rad} + C_{\rm vdW}\left(\frac{n_{\rm H\,I}}{10^{16}}\right)\left(\frac{T}{5000}\right)^{0.3} + C_{\rm Stark}\left(\frac{n_e}{10^{12}}\right) + C_{\rm res}\left(\frac{n_{\rm H1}}{10^{16}}\right), \quad (1)$$

where $n_{\rm H\,I}$ is the neutral hydrogen density, $n_{\rm H1}$ is the density of the hydrogen ground state, T is the electron temperature in kelvins, and n_e is the electron density.

2.2. *Helium*

We use a five-level helium atom in these calculations as listed in Table 4, which tabulates the same parameters as Table 1. The photoionization cross sections tabulated are from Mathisen (1984). Collisional rate coefficients for our helium atomic model can be found in Table 5, and Einstein A-values

TABLE 4

PHOTOIONIZATION DATA FOR THE NEUTRAL HELIUM ATOMIC MODEL

Level (i)	Notation	g_i	λ_i (Å)	σ_i (10^{-18} cm²)
1........	$1s^2\ ^1S$	1	504.27	7.376
2........	$2s\ ^3S$	3	2600.85	5.496
3........	$2s\ ^1S$	1	3122.31	9.237
4........	$2p\ ^3P^o$	9	3422.56	16.3
5........	$2p\ ^1P^o$	3	3680.55	13.8

TABLE 5

COLLISIONAL RATE COEFFICIENTS FOR THE HELIUM ATOMIC MODEL

A. IONIZATION: $\Omega_i(T)$ (cm³ s⁻¹)

Level (i)	4000 K	8000 K	15,000 K	20,000 K	40,000 K
1............	1.45(−9)	2.05(−9)	2.83(−9)	3.29(−9)	4.08(−9)
2............	1.51(−8)	2.19(−8)	3.16(−8)	3.76(−8)	5.71(−8)
3............	2.07(−8)	3.02(−8)	4.39(−8)	5.23(−8)	7.88(−8)
4............	1.58(−8)	2.33(−8)	3.39(−8)	4.04(−8)	6.05(−8)
5............	1.85(−8)	2.73(−8)	3.98(−8)	4.75(−8)	7.07(−8)

B. EXCITATION: $\Omega_{ji}(T)$ (cm³ s⁻¹)

Transition	4000 K	8000 K	15,000 K	20,000 K	40,000 K
2–1.........	9.24(−9)	7.00(−9)	5.37(−9)	4.80(−9)	3.64(−9)
3–1.........	4.39(−9)	3.87(−9)	3.61(−9)	3.53(−9)	3.16(−9)
3–2.........	1.07(−7)	8.07(−8)	6.12(−8)	4.98(−8)	2.72(−8)
4–1.........	1.47(−9)	1.62(−9)	1.73(−9)	1.72(−9)	1.51(−9)
4–2.........	4.97(−7)	7.52(−7)	1.00(−6)	1.16(−6)	1.50(−6)
4–3.........	1.89(−7)	1.52(−7)	1.29(−7)	1.15(−7)	7.80(−8)
5–1.........	1.19(−9)	1.58(−9)	2.01(−9)	2.16(−9)	2.55(−9)
5–2.........	3.03(−8)	3.00(−8)	2.78(−8)	2.60(−8)	1.92(−8)
5–3.........	9.45(−7)	1.49(−6)	1.83(−6)	2.03(−6)	2.37(−6)
5–4.........	5.12(−8)	4.10(−8)	3.57(−8)	3.25(−8)	2.06(−8)

TABLE 6
EINSTEIN A-VALUES AND LINE BROADENING HALF-WIDTHS FOR THE
HELIUM ATOMIC MODEL

Transition	λ_{vac} (Å)	A (10^7 s^{-1})	C_{rad} (10^{-5} Å)	C_{vdW} (10^{-5} Å)	C_{Stark} (10^{-5} Å)
4–2	10832.98	1.02	3.18	42.1	0.54
5–1	584.33	180.	1.628	0.271	0.163
5–3	20585.87	0.1976	2030.	59.0	3.75

and line-broadening half-widths are listed in Table 6. We include the following collisional transitions: 2–1, 3–1, 3–2, 4–1, 4–2, 4–3, 5–1, 5–2, 5–3, and 5–4, where the 2–1, 3–1, 4–1, and 5–1 coefficients are obtained from Aggarwal, Kingston, & McDowell (1984) and the 3–2, 4–2, 4–3, 5–2, 5–3, and 5–4 coefficients are from Mendoza (1983). Einstein A-values for our radiative transitions—4–2, 5–1, and 5–3—are obtained from Kono & Hattori (1984). Finally, Stark half-widths are from data published by Dimitrijevic & Sahal-Bréchot (1984). Equation (1) is also used to determine the total half-width for the helium transitions without the inclusion of the resonance broadening. We used only the five lowest energy levels of neutral helium for these model atmospheres since the temperatures at all depths are typically below 10^4 K, and essentially all He atoms are found in the He I ground state. Singly ionized helium calculations are not made since this ionic stage is negligible relative to the neutral helium density and the ionized hydrogen density.

3. HYDROGEN IONIZATION AND EXCITATION

A series of radiative transfer calculations are made for various atmospheric models of cool giant stars under various radiative transfer assumptions. All calculations assume a plane-parallel, static medium. Table 7 displays the characteristics of each run: the model used, the star it represents, and any assumptions made in the radiative transfer. From a model atom of three bound levels, number densities and departure coefficients are determined explicitly for the first three levels. Hydrogen bound-free opacities for the lowest eight energy levels are included in the background continuum calculations. Number densities for levels $n = 4$ to $n = 8$ are determined as follows. The departure coefficients for level 8 are set to unity at all depths, and departure coefficients for levels between level 3 and level 8 are linearly interpolated as a function of level number. The number densities for levels 4–8 are then determined from these departure coefficients and calculated LTE populations. In all cases, however, as can be judged from Figures 2–4, the population of these levels is so low that their bound-free opacities are negligible.

The statistical equilibrium equations for this three-level hydrogen model are

$$n_i \sum_{j=1(\neq i)}^{3} [P_{ij} + P_{i\kappa}] = \sum_{j=1(\neq i)}^{3} [n_j P_{ji} + n_\kappa P_{\kappa i}] \qquad (2)$$

and

$$n_\kappa \sum_{i=1}^{3} P_{\kappa i} = \sum_{i=1}^{3} n_i P_{i\kappa} , \qquad (3)$$

where n_i represents the number density in bound level i, n_κ represents the continuum (i.e., ion) number density, and P represents the total transition rate (radiative R plus collisional C) between the respective states. The photoionization rate is determined from

$$R_{i\kappa} = 4\pi \int_{\nu_{\kappa 1}}^{\infty} \frac{1}{h\nu} \alpha_i(\nu) J_\nu \, d\nu , \qquad (4)$$

TABLE 7
MODEL PARAMETERS

Model[a]	T_{eff}	log g	C/O	Type[b]	Star	T_{rad}[c] (Balmer)	m^d (Balmer)	T_{rad}[c] (Paschen)	m^d (Paschen)
A1						2800	88.	3000	270.
A2	3200	0.0	0.58	Ph	g Her	2920	4.8	2820	15.
A3						2920	4.8	2820	15.
B1						2600	610.	2800	770.
B2	3000	0.0	1.05	Ph	TX Psc	2740	5.4	2490	120.
B3						2740	5.4	2490	120.
C1						2700	130.	2900	350.
C2	3100	−0.5	1.03	Ph	TX Psc	2780	5.8	2770	34.
C3						2780	5.8	2770	34.
D1						2800	88.	3000	270.
D2						2900	0.56	2810	4.8
D3	3200	0.0	0.58	Ch	g Her	2900	0.56	2810	4.8
D4						2900	0.56	2810	4.8
E1						2600	610.	2800	880.
E2						2710	0.86	2440	5.4
E3	3000	0.0	1.05	Ch	TX Psc	2710	0.86	2440	5.4
E4						2710	0.86	2440	5.4

NOTE.—All temperatures are in kelvins.
[a] Key to model labels: (1) Detailed balance in the Lyman lines. (2) All transitions handled in detail, line transitions in CRD. (3) Same as (2), except He I NLTE calculations are included. (4) Same as (3), except Lyα calculated in PRD.
[b] Ph = pure photospheric model; Ch = chromospheric-photospheric model.
[c] Radiation temperatures for the Balmer and Paschen continua in the outer layers.
[d] Layers above the tabulated column mass (g cm^{-2}) have contant Balmer and Paschen continua radiation temperatures. See text for further details.
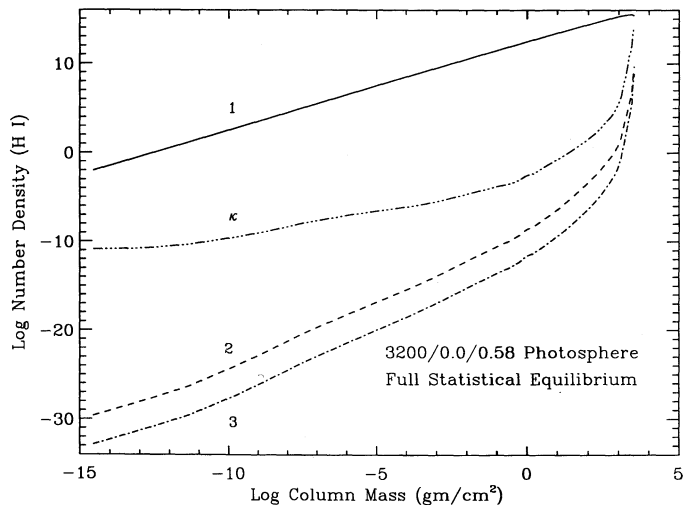
FIG. 2.—Ionization and excitation for a photospheric model of an M giant star. Results for the number density of the atoms in the states $n = 1, 2, 3$, and κ (continuum = ion) for H I are shown with full statistical equilibrium in the solution of the radiative transfer equation of the Lyman lines. Note that electron densities used in the LTE calculations are those derived from the statistical equilibrium equations.

and the radiative recombination rate (per ionized atom) is

$$R_{\kappa i} = \frac{n_i^*}{n_\kappa^*} R_{i\kappa}^\dagger , \qquad (5)$$

where

$$R_{i\kappa}^\dagger = 4\pi \int_{\nu_{\kappa 1}}^\infty \frac{1}{h\nu} \alpha_i(\nu) e^{-h\nu/kT} \left(\frac{2h\nu^3}{c^2} + J_\nu \right) d\nu . \qquad (6)$$

The thermodynamic-equilibrium ratio n_i^*/n_κ^* is given by the Saha-Boltzmann equation with a value of n_e derived from the statistical equilibrium equations. Collisional ionizations are calculated via

$$C_{i\kappa} = n_e \Omega_i(T) e^{-k\nu_{\kappa i}/kT} , \qquad (7)$$
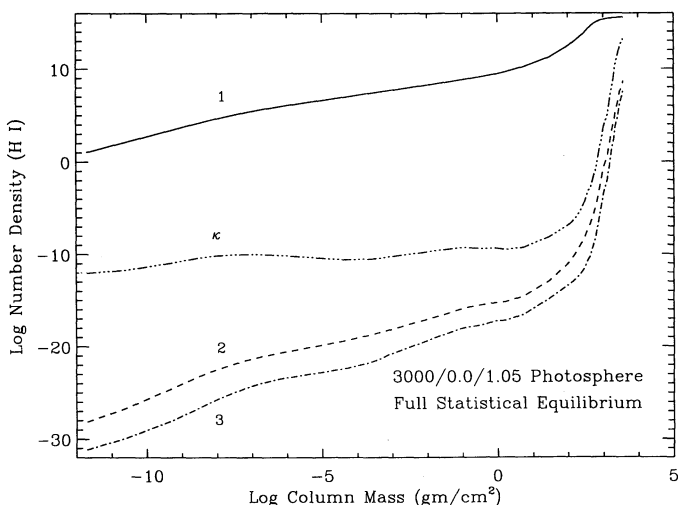
FIG. 3.—Ionization and excitation for a photospheric model of a cool carbon star (Johnson 1982) as in the LJAL model (see text). Results for the number density of the atoms in the states $n = 1, 2, 3$, and κ (continuum = ion) for H I are shown with full statistical equilibrium in the solution of the radiative transfer equation of the Lyman lines.
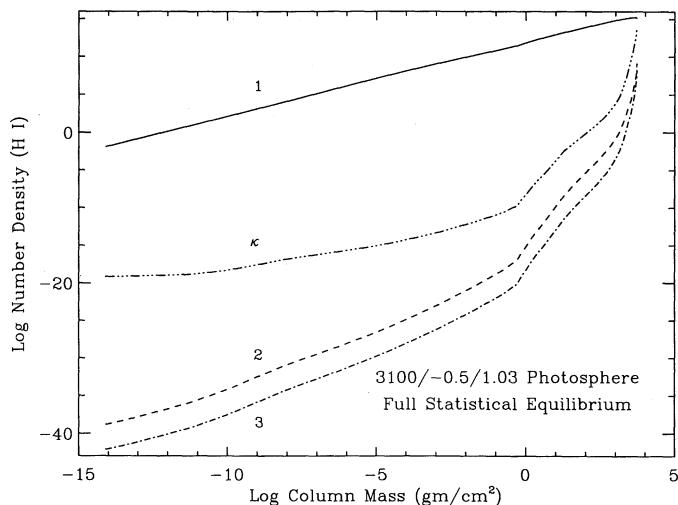

FIG. 4.—Ionization and excitation for a photospheric model of a cool carbon star computed with polyatomic as well as diatomic molecular opacities (Jørgensen 1989). Results for the number density of the atoms in the states $n = 1, 2, 3$, and κ (continuum = ion) for H I are shown with full statistical equilibrium in the solution of the radiative transfer equation of the Lyman lines.

where Ω_i is the collisional coefficient or collisional *strength* tabulated in Table 2. Only electronic collisions are included in these ratios; inelastic collisions by neutral atoms are not considered. Since collisional transitions are in detailed balance with the equilibrium densities, the collisional recombinations are determined from

$$C_{\kappa i} = \frac{n_i^*}{n_\kappa^*} C_{i\kappa} . \qquad (8)$$

In these atmospheric models, collisional ionizations and recombinations are negligible with respect to photoionizations and photorecombinations due to the low electron and atomic densities. The Lyman-continuum transfer equation is handled separately from all other bound-free opacities, and the method used to solve this equation is described in detail in Appendix C of VAL III.

The total bound-bound rates for a given transition is the sum of the radiative rates plus collisional rates. The net radiative rate is defined as

$$n_j R_{ji} - n_i R_{ij} = n_j A_{ji} \rho_{ji} \quad (j > i) , \qquad (9)$$

where $R_{ji} = A_{ji} + B_{ji} \bar{J}_{ji}$ is the radiative transition rate from level j to level i; $R_{ij} = B_{ij} \bar{J}_{ji}$ is the radiative rate in the reverse direction; A_{ji}, B_{ji}, and B_{ij} are the Einstein coefficients; $\bar{J}_{ji}$ is the total amount of radiation in the line; and ρ_{ji} is the net radiative bracket. Meanwhile, collisional excitation rates are calculated from

$$C_{ij} = n_e \Omega_{ji}(T) e^{-h\nu_{ji}/kT} , \qquad (10)$$

where Ω_{ji} is the collisional excitation coefficient of Table 2. Collisional de-excitation are handled in the same manner as collisional recombinations, except j replaces κ in equation (8).

The frequency-independent source function of the bound-bound transition can be written in the form (e.g., VAL I)

$$S_{ji} = \frac{2h\nu_{ji}^3/c^2}{(g_j/g_i)(n_i/n_j) - 1} , \qquad (11)$$

where g_j and g_i are the statistical weights of the upper and lower states, respectively. From equations (9) and (11), we can rewrite the net radiatives bracket as

$$\rho_{ji} = 1 - \bar{J}_{ji}/S_{ji} . \quad (12)$$

Note that the description of the source function above is assumed to be frequency-independent; a description of the source function calculation under the assumption of partial redistribution can be found in Appendix A of VAL III. A more detailed description of this equivalent two-level atom approach to the solution of the coupled equations of radiative transfer and statistical equilibrium can be found in VAL I and VAL III.

3.1. *Photospheric Models*

We begin by investigating NLTE effects in the level populations of the first three levels of hydrogen for *pure* photospheric models representative of two selected late-type giant stars, g Her (M6 III) and TX Psc (C6, 2), which together include many of the interesting features of very late-type giants. The models are shown in Figure 1. By "pure," we mean that the model is described solely with a positive temperature (T) gradient with respect to column mass (m) as deduced via the assumption of radiative, or radiative plus convective, equilibrium. After investigating NLTE effects from the photospheric radiation field, we attach a semiempirical "chromospheric" temperature rise (i.e., $dT/dm < 0$) to the outer layers of the photospheric models to determine NLTE effects at chromospheric depths and NLTE effects in the photosphere from backflowing chromospheric radiation.

The first round of calculations made the assumption of *detailed balance* (DB) in the Lyman lines (i.e., models A1, B1, and C1). The assumptions of DB in bound-bound transitions implies $n_i R_{ij} = n_j R_{ji}$ or $\rho_{ji} = 0$. This assumption is often valid at large optical depths, where $\bar{J}_{ji}$ *may* be essentially equal to S_{ji}. The hydrogen Lyman lines are always optically thick in late-type stars, so as a starting point, we make this assumption. Our initial calculations also assume $J_\nu = W(m)B_\nu[T_{rad}(m)]$ for the hydrogen Balmer and Paschen continua, where $W(m)$ is the geometric dilution factor. We take $W = 0.5$ depths with $m < 1$ g cm^{-2} and $W = 1$ for depths with $T > T_{eff}$, and W is linearly interpolated with respect to depth points between these limits. The Balmer and Paschen radiation temperatures are given in Table 7 for each model (A1, B1, C1) and used at depths where $T_e < T_{rad}$, while $T_{rad} = T_e$ for $T_e \geq T_{rad}$. The Lyman photoionization rate is handled in detail. After convergence is achieved, we then allow the Lyman lines to radiate and handle the Balmer and Paschen ionization in detail (i.e., models A2, B2, and C2), the so-called *full statistical equilibrium* (FSE) case, to investigate the effect the DB approximation has on the excitation and ionization of hydrogen. Table 7 also lists the actual radiation temperatures for the FSE calculations of the Balmer and Paschen photoionization rates for comparisons with the assumed radiation temperatures in the DB calculations. Later, the FSE calculations are repeated for hydrogen when helium densities are determined from NLTE analyses (i.e., models A3, B3, and C3) in order to determine helium's effect on the hydrogen ionization and excitation. In all of our pure photospheric models, NLTE effects on He I populations have no effect on the hydrogen ionization and excitation.

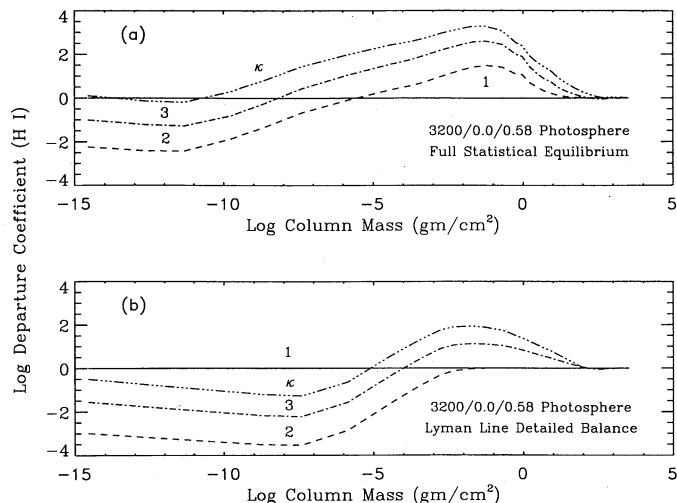Figures 2, 3, and 4 show the hydrogen bound levels and ion

FIG. 5.—Ionization and excitation for a photospheric model of an M giant star. The departure coefficients of H I are shown (*a*) with full statistical equilibrium in the solution of the radiative transfer equation of the Lyman lines and (*b*) under the assumption of detailed balance in the Lyman lines. Note that electron densities used in the LTE calculations are those derived from the statistical equilibrium equations.

densities as a function of column mass for the g Her photospheric model and the two TX Psc photospheric models, respectively. Meanwhile, Figures 5, 6, and 7 display the departure coefficients with respect to LTE corresponding to Figures 2, 3, and 4, respectively. In addition, these departure coefficient figures show a comparison between the results obtained for the FSE calculations (*top*) and the DB calculations (*bottom*). We define the departure coefficient as $b_i \equiv n_i/n_i^*$, where the * represents LTE values (note that some authors define b_i as $[n_i/n_i^*]/[n_\kappa/n_\kappa^*]$, e.g., VAL I, II, III), The LTE ion densities are determined here via the Saha equations based on electron densities calculated from our NLTE analysis.
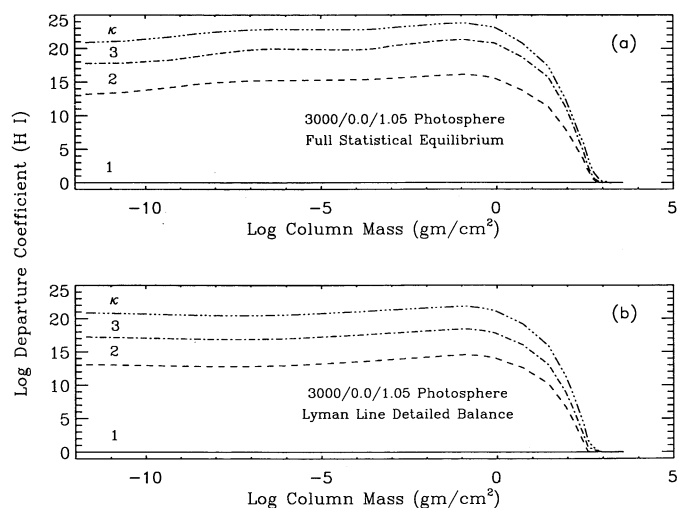

FIG. 6.—Ionization and excitation for a photospheric model of a cool carbon star (Johnson 1982) as in the LJAL model (see text). The departure coefficients of H I are shown (*a*) with full statistical equilibrium in the solution of the radiative transfer equation of the Lyman lines and (*b*) under the assumption of detailed balance in the Lyman lines.
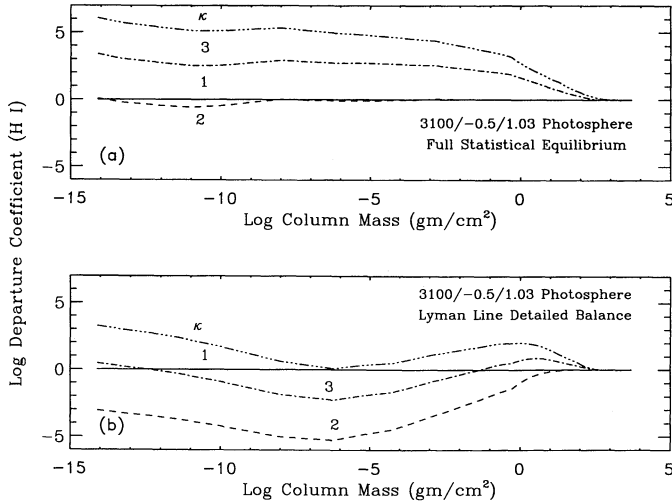
FIG. 7.—Ionization and excitation for a photospheric model of a cool carbon star computed with polyatomic as well as diatomic molecular opacities (Jørgensen 1989). The departure coefficients of H I are shown (a) with full statistical equilibrium in the solution of the radiative transfer equation of the Lyman lines and (b) under the assumption of detailed balance in the Lyman lines.

Several points are raised by these population figures; we shall address those concerning the ionization equilibrium first.

1. Hydrogen is neutral by a large factor throughout the photosphere, the degree of ionization being miniscule.

2. Due to the large reservoir of hydrogen atoms in the ground state, $b_1 = 1$ at all depths for these photospheric models.

3. Hydrogen begins to overionized *with respect to LTE* (though still neutral by a large factor) in the photospheric models at depths just above the continuum formation region ($m \approx 10^3$ g cm^{-2}), due in part to the tiny amount of ionized hydrogen in LTE. The ionization equilibrium, with respect to column mass, behaves differently for each model and for the assumptions used in the Lyman lines radiative transfer.

4. In the 3200/0.0/0.58 (A) model, this hydrogen overionization reaches a peak just above $m = 0.1$ g cm^{-2} and then begins to decrease at higher depths. This phenomenon is not represented to the same extent in the carbon star models.

5. Hydrogen in the 3000/0.0/1.05 (B) model is still almost entirely neutral but is fantastically overionized (by a factor 10^{20}!) relative to LTE, and this ionization remains fairly constant with depth. This strikingly large overionization of a neutral element arises from the incredibly low ion density expected in LTE in this cool gas.

6. The model with 3100/−0.5/1.03 (C) also shows an enormous overionization (a factor of ~10^5 at the peak), and this rises sharply at depths just above the region of formation of the visual continuum as in models A and B. The overionization with respect to LTE is not as great in this model as compared to model B due to the temperature-density structure differences between this "polyatomic molecular" model C and the "diatomic molecular" model B. The inclusion of polyatomic molecular opacities in radiative equilibrium models lower the pressure with respect to the Rosseland mean optical depth in the upper layers due to an expansion of the model with respect to models converged with only diatomic molecular opacities (Jørgensen et al. 1985). This results in warmer upper layers with respect to column mass (and gas density) as can be seen in

Figure 1a. As such, for a given column mass T(polyatomic model) > T(diatomic model), which gives rise to an enhanced LTE ionized hydrogen density hence reducing b_κ in the outer layers of model C with respect to model B.

7. In all cases, the Lyman line DB calculations (the lower panel of Figs. 5, 6, and 7) predict that hydrogen is underionized with respect to those cases where all lines are handled in detail (i.e., FSE). Indeed, the Lyman-line detail balance calculation becomes "underionized" with respect to LTE at depths $m < 10^{-5}$ g cm^{-2} in model A2 (see Fig. 5). We stress here that even though hydrogen is strongly overionized with respect to LTE, *the proton density is exceedingly small with respect to the total hydrogen density*; in the upper photosphere ($m < 1$ g cm^{-2}) of our radiative equilibrium models, $n_p/n_H \sim 10^{-9}$ to 10^{-16} (model A2), $\sim 10^{-21}$ to 10^{-14} (models B2 and C2).

An examination of the excitation equilibrium in these cool stellar photospheres reveals the following:

8. As with the ionization equilibrium, the bound levels are overexcited with respect to LTE in the FSE calculations, except for the uppermost layers of the g Her radiative equilibrium model.

9. Lyman line detailed balance causes a "de-excitation" with respect to FSE calculations.

Points (1) and (2) above are easily understood by examining Figures 1a and 1b and noting the cool temperatures throughout these radiative equilibrium atmospheres. The extreme overionization of hydrogen with respect to LTE (points [3]–[6]) can be demonstrated by examining the *detailed* ionization/recombination processes for these models. This analysis also leads to an explanation of the effect that Lyman line detailed balance has on the ionization (point [7]) and the excitation (points [8] and [9]) equilibria. We demonstrate the controlling mechanisms of these processes by using equations (2) and (3) to solve for the ratio n_κ/n_1, where $n_\kappa = n_p$ for hydrogen. The solution for this ratio is long and cumbersome even for a simple three-level atom (e.g., Avrett 1968). However, physical insight to this problem can still be gained using a two-level atom. For a two-bound level–plus–continuum hydrogen atomic model, equations (2) and (3) become

$$\frac{n_\kappa}{n_1} = \frac{R_{1\kappa} + (n_2/n_1)R_{2\kappa}}{R_{\kappa 1} + R_{\kappa 2}}$$

$$= \frac{R_{1\kappa} + R_{2\kappa}[Z_{12}/(A_{21}\rho_{21} + Z_{21})]}{R_{\kappa 1} + R_{\kappa 2}}, \qquad (13)$$

where

$$Z_{ij} = C_{ij} + \mathscr{P}_{ij}, \qquad (14)$$

C_{ij} are the bound-bound collisional rates, $\mathscr{P}_{ij}$ are indirect transitions between two bound levels through the continuum, the so-called *bound-free-bound* rates, and are given by

$$\mathscr{P}_{ij} = \frac{P_{i\kappa}P_{\kappa j}}{\Sigma_m P_{\kappa m}}. \qquad (15)$$

The assumption of detailed balance in Lyα then gives

$$\frac{n_\kappa}{n_1} = \frac{R_{1\kappa} + R_{2\kappa}(Z_{12}/Z_{21})}{R_{\kappa 1} + R_{\kappa 2}}. \qquad (16)$$

At this point, we split the radiative equilibrium models into two regions: the *upper photosphere*, as defined by depths with

$m < 1$ g cm^{-2}; and the *lower photosphere*, as defined by depths with $m > 1$ g cm^{-2}. We now examine each model separately since each has unique characteristics in ionization an excitation equilibria.

3.1.1. *Models A*: 3200/0.0/0.58 (*g Her*)

We compare the various rates of equations (13) and (16) at different regions in the atmosphere. For the Lyman line DB calculations (model A1), equation (16) is used, where

$$\frac{n_2}{n_1} = \frac{Z_{12}}{Z_{21}} \approx \frac{\mathscr{P}_{12}}{\mathscr{P}_{21}} \qquad \text{(upper photosphere, Ly}\alpha\text{ DB)}$$

$$\approx \frac{C_{12} + \mathscr{P}_{12}}{C_{21} + \mathscr{P}_{21}} \qquad \text{(lower photosphere, Ly}\alpha\text{ DB)} .$$

$$(17)$$

A curious result is found with this assumption of Lyman-*line* detailed balance: $n_1 R_{1\kappa} = n_\kappa R_{\kappa 1}$, even though the Balmer ionization and recombination terms in equation (16) are *not* negligible with respect to the Lyman continua rates. Lyman-*continuum* detailed balance becomes valid under the Lyman line detailed balance aproximation due to the fact that $R_{1\kappa}/(Z_{12}/Z_{21})R_{2\kappa} \approx R_{\kappa 1}/R_{\kappa 2}$ to within 1% or better at each depth, and that this ratio varies with depth by only 30% over the entire atmosphere (3.4 at the top of the atmosphere to 2.4 at the base). This coincidence can be understood by realizing that photoionizations and photorecombinations dominate bound-bound collisional rates in the upper photosphere. Using equations (15) and (17) in equation (16), we get

$$\frac{n_\kappa}{n_1} \approx \frac{R_{1\kappa} + R_{2\kappa}[(R_{1\kappa} R_{\kappa 2}/\Sigma_m R_{\kappa m}) \cdot (\Sigma_m R_{\kappa m}/R_{2\kappa} R_{\kappa 1})]}{R_{\kappa 1} + R_{\kappa 2}}$$

$$\approx \frac{R_{1\kappa} + R_{1\kappa}(R_{\kappa 2}/R_{\kappa 1})}{R_{\kappa 1} + R_{\kappa 2}} = \frac{R_{1\kappa}(1 + R_{\kappa 2}/R_{\kappa 1})}{R_{\kappa 1}(1 + R_{\kappa 2}/R_{\kappa 1})}$$

$$\approx \frac{R_{1\kappa}}{R_{\kappa 1}} \qquad \text{(upper photosphere, Ly}\alpha\text{ DB)} ; \qquad (18)$$

hence Lyman-continuum detailed balance is recovered. In the lower photosphere, radiation temperatures become equivalent to electron temperatures which forces the ratios of the terms in the numerator of equation (16) to be similar to the ratio of the terms in the denominator. The overionization with respect to LTE can now be understood through the interaction of the ground state with the excited levels through the bound-free-bound rates: as an electron is ionized out of the ground state, a significant fraction recombine through the upper levels. The Balmer and Paschen continua are optically thin throughout the entire atmosphere, so that as the electrons cascade back down toward the ground state, they "see" the photospheric radiation field of where the various continua thermalize [i.e., $S_\nu = B_\nu(\tau_\nu \approx 1)$]. For this g Her photospheric model, the strongest opacity sources at the continuum formation depth are H Rayleigh scattering (40%), H$^-$ bound-free (28%), and Mg I bound-free (28%) for the Balmer-continuum bound-free edge spectral region, and H$^-$ bound-free (97%) for the Paschen-continuum bound-free edge region. This demonstrates that the "on-the-spot" approximation for the Lyman continuum (i.e., each internally produced Lyman-continuum photon is absorbed locally, *solely* by the Lyman continuum such that $T_{\rm rad} \approx T_e$), which is often used in low-density environments, is not valid where substantial visual and infrared radiation fields exist, due to interactions with higher lying levels.

Relaxing the assumption of detailed balance in Lyα (model A2), one must now compare the net radiative rate to the collisional rates for this transition and the bound-free-bound rates. In the upper photospheric regions of these models, $|A_{21} \rho_{21}| \sim Z_{21} (\approx \mathscr{P}_{21})$, while at lower photospheric depths ($m > 10$ g cm^{-2}) $|A_{21} \rho_{21}| \ll Z_{21}$. This shows the validity of Lyman line detailed balance deep in the photospheres ($m > 10$ g cm^{-2}) where collisional and bound-free-bound rates begin to exceed greatly the net radiative rates. Allowing the Lyman lines to radiate also invalidates the Lyman continuum DB approximation in the upper photosphere. Our guess of the Balmer radiation temperature in the Lyman line DB calculations leads to a factor of 4 decrease in the Balmer photoionization rate, which should give a slight overionization with respect to the FSE calculations—just the opposite of what is observed. The main contributor to the differences in the ionization equilibrium between the FSE and Lyman line DB calculations is the radiative transfer in the Lyman lines themselves. The net radiative bracket is negative (i.e., more absorptions than emissions) and comparable to the other rates for $m < 1$ g cm^{-2} which acts as a "pump" to further excite the upper levels through the Lyman bound-bound transitions. Once excited, the electrons "see" the deep photospheric radiation field, enhanced by the Planck function reaching a maxima in the infrared, and immediately ionize. As a result, the Lyman line DB approximation leads to an underexcitation and underionization with respect to FSE calculations due to the fact the "Lyman-pump" is "turned off." Examinations of equation (12) displays the reason for the negative net radiative rates for the Lyman lines in the upper regions of this photospheric model: $\bar{J}_{ji} > S_{ji}$ due to the local Planck function being so much smaller than the mean intensity, since S_{ji} depends on a weighted combination of $\bar{J}_{ji}$ and $B_{ji}(T)(\ll \bar{J}_{ji})$, the Planck function at line center. Although the Lyman lines are dominated by scattering processes in the upper layers of these models, there are sufficient numbers of absorptions to force $S_{ji} < \bar{J}_{ji}$, which enhances the number densities in the excited levels under the assumption of full statistical equilibrium with respect to the assumption of DB in the Lyman lines.

3.1.2. *Models B*: 3000/0.0/1.05 (*TX Psc*)

We now examine the various rates in equations (13) and (16) for the B models. Once again the Lyman line DB approximation forces the Lyman continuum into detailed balance, with one interesting exception: The Lyman continuum goes out of detailed balance in the molecular hydrogen formation region ($10 < m < 300$ g cm^{-2}). Relaxing the Lyman line DB approximation causes the Lyman continuum to go out of detailed balance. The Balmer radiation temperature guess for the photoionization rate underestimates $R_{2\kappa}$ by a factor of 5 in this model. For this TX Psc photospheric model, the strongest opacity sources at the continuum formation depth are H$_2$ Rayleigh scattering (38%), H$^-$ bound-free (33%), H Rayleigh scattering (21%), and Mg I and Na I bound-free (3% each) for the Balmer-continuum bound-free edge spectra region, and H$^-$ bound-free (98%) for the Paschen bound-free edge. Again, the assumption of Lyman line detailed balance is valid deep in the photosphere ($m > 10^3$ g cm^{-2}) due to the increased collisional rates with respect to the net radiative rates. The *underionization* of hydrogen in the upper photosphere *under the assumption of detailed balance* in comparison to the FSE calculations is

obvious from equations (13) and (16) and

$$\frac{n_2}{n_1} \approx \frac{\mathscr{P}_{12}}{A_{21}\rho_{21} + \mathscr{P}_{21}} \qquad \text{(upper photosphere, FSE)}$$

$$\approx \frac{\mathscr{P}_{12}}{A_{21}\rho_{21} + C_{21} + \mathscr{P}_{21}} \qquad \text{(lower photosphere, FSE)}$$

$$\approx \frac{C_{12} + \mathscr{P}_{12}}{C_{21} + \mathscr{P}_{21}} \qquad (m > 10^3 \text{ g cm}^{-2}, \text{FSE}) .$$

(19)

Since the net Lyα rate is negative throughout much of this atmosphere, n_κ/n_1 is smaller under the assumption of Lyman line detailed balance. Essentially, the transfer of radiation in the Lyman lines, particularly Lyα, controls the ionization equilibrium of hydrogen in late-type giants. Once again, the net radiative bracket becomes negative due to $\bar{J}_{ji} > S_{ji}$.

3.1.3. Models C: 3100/−0.5/1.03 (TX Psc)

Once again we compare the radiative and collisional rates of equations (13) and (16) for the C models. Detailed balance in the Lyman lines is a valid assumption deep in the photosphere ($m > 100$ g cm^{-2}) due to the increased collisional rates with respect to the net radiative rates and bound-free-bound rates. Lyman line DB once again forces the Lyman continuum into detailed balance to within 4%. Our guess of $T_{\rm rad}$ for the Balmer photoionization underestimates this rate by a factor of 3. Lyman line DB again causes an underionization and underionization and underexcitation with respect to FSE calculations.

The fundamental difference between the two carbon star models is the temperature distribution with respect to the total hydrogen density. As previously mentioned, the inclusion of polyatomic molecular opacities in radiative equilibrium calculations lowers the density in the $T(m)$ [or $T(P)$] grid as compared to an atmosphere converged with only diatomic molecular opacities. Because of this, collisional rates are much less in the B models in comparison to the C models, which enables radiative processes to dominate far deeper into the atmosphere and causes J_ν to be many orders of magnitude different from B_ν. The level and ion densities in the diatomic molecular models are determined essentially by the radiation field of the deep photosphere and virtually do not "see" the local conditions of the gas. The g Her photosphere is also based upon polyatomic opacities, which lends itself to a comparison with the polyatomic carbon star model. A reexamination of Figures 5 and 7 shows that the functional "shape" of the departure coefficients for the Lyman line DB calculations are similar, the main differences arising from the factor of 10 increase in collisional rates in the oxygen-rich model. The full statistical equilibrium calculations are fundamentally different in these two models—the 3200/0.0/0.58 model departure coefficients reach a maximum value near log $m = -1.5$ and then decrease with decreasing column mass, which is not seen (perhaps just barely) in the 3100/−0.5/1.03 model. This results from the enhanced carbon density in the carbon star: The strongest bound-free opacity under the Lyman lines is from neutral carbon (except Lyα, where Si I b-f dominates but C I is still substantial); the enhanced carbon abundance increases the C I b-f opacity and the continuum source function, which in turn, lowers the net radiative rate in the outer regions of the carbon star atmosphere (model C2) via equation (12). Hence

the oxygen-rich model has greater negative net radiative rates in the Lyman lines in comparison to the carbon-rich model which *drains* the excited and ion states to a larger extent in model A2 in comparison to model C2. *Carbon abundance has a significant effect on both the ionization and excitation of hydrogen.* Since radiative transfer effects in Lyα dominate the other Lyman lines and Si I is the strongest bound-free opacity under Lyα, nonsolar silicon abundances should also have a major impact on the ionization and excitation of hydrogen. This should be of fundamental importance in the analysis of planetary nebulae, H II regions, and active galactic nuclei, where both carbon and silicon abundances may be quite different from solar values.

3.2. Photospheric plus Chromospheric Models

IUE spectra of late-type stars show evidence of chromospheric emission in singly ionized metal lines. It is still unclear in the non-Mira variables of the nature of the "chromospheres" of these stars. Chromospheres have been modeled for g Her and TX Psc based on the Mg II h and k lines from a semi-empirical approach (LJE 1992 and LJAL 1989, respectively). We now investigate the effect a chromospheric radiation field has on the ionization and excitation equilibrium of cool giant stars.

3.2.1. The g Her Model

Figures 8a and 8b compare the number densities of the first three bound levels and the ion of hydrogen for the full statistical equilibrium calculations of the chromospheric-photospheric model (D2) and the pure photospheric model (A2) of g Her. Figures 9a and 9b are the corresponding plots of the departure coefficients. Before commenting on the analysis of these figures, we first discuss the assumption of Lyman line DB in this chromospheric-photospheric model of g Her. Hydrogen is *overionized* and *overexcited* at chromospheric depths with the Lyman lines in DB as compared to calculations where the lines are handled in detail. Meanwhile, in the upper photosphere ($T_{\min} \leq T < T_{\rm eff}$), just the reverse is true; Lyman line detailed balance predicts an *underionization* and *underexcitation* of hydrogen in comparison to calculations
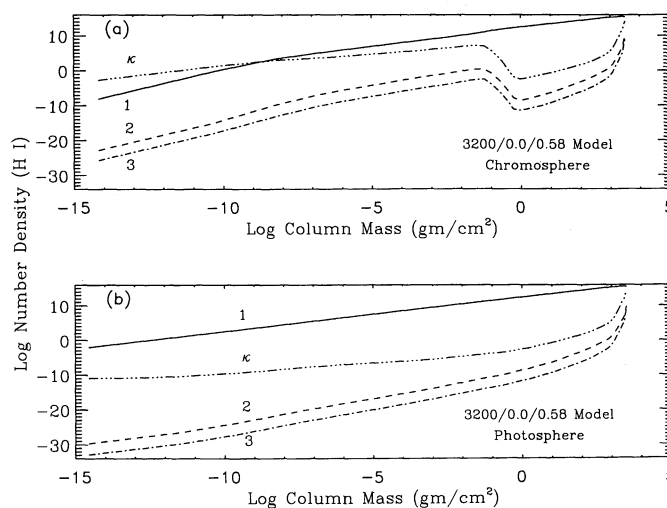

FIG. 8.—Effect of a chromosphere. Plotted are the number densities of the atoms in the states $n = 1, 2, 3$, and κ (continuum = ion) for H I with full statistical equilibrium of the Lyman lines for either (a) a photosphere plus chromosphere or (b) a photosphere only, for the star g Her (M6 III).
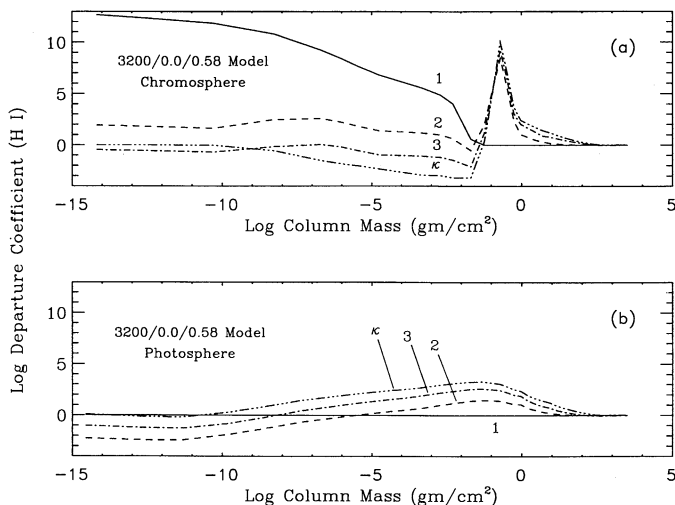
FIG. 9.—Effect of a chromosphere, The departure coefficients corresponding to the number densities of Fig. 8 for the atoms in the states $n = 1, 2, 3$, and κ (continuum = ion) for H I with full statistical equilibrium of the Lyman lines for either (a) a photosphere plus chromosphere or (b) a photosphere only, for the star g Her (M6 III).

where the Lyman lines are handled in detail. Once again, as was the case for the pure photospheric models, the Lyman lines are affecting both the excitation and ionization of hydrogen. At photospheric depths ($m > 0.2$ g cm^{-2}), the net radiative bracket is negative (i.e., more absorptions than emissions, $\bar{J}_{ji} > S_{ji}$) and comparable to the other rates, which, like the pure photospheric models, acts as a "pump" to further excite the upper levels through the Lyman bound-bound transitions. While at chromospheric depths ($m < 0.2$ g cm^{-2}), the net radiative bracket is positive (i.e., more emissions than absorptions, $\bar{J}_{ji} < S_{ji}$) and dominates the collisional and photoionization rates. The Lyman lines act as a "drain" for the excited levels in the chromosphere and a "pump" in the upper photosphere.

Another interesting phenomena is the effect that backflowing chromospheric radiation has on the ionization and excitation at photospheric depths near the temperature minimum region (see Fig. 8). The ionization and excitation is a factor of 20 greater in a region in the photosphere just below the chromosphere as compared to the same column mass in the pure photosphere model ($0.2 < m < 0.8$ g cm^{-2}). The Lyman continuum in the temperature minimum region "sees"

radiation from below plus the enhanced ultraviolet flux from the chromosphere above. This may seem intuitively incorrect, since the Lyman continuum is very optically thick in this region ($\tau_{L\kappa} = 10^7$–10^8). However, it is the Lyman lines that are controlling the ionization and excitation. The Lyman lines are very optically thick as well ($\tau_{L\alpha} = 10^9$–10^{10}); however, the extreme line wings are *not*. Both C I and Si I bound-free opacities are large under Lyα, and they remain optically thick into the chromosphere (i.e., the continuum depth of formation at the Lyα and Lyβ transitions are both in the lower chromosphere). As such, the flux from these opacities is enhanced in the T_{min} regime of the chromospheric-photospheric model as compared to similar depths in the pure photospheric model. Since the Lyman lines (actually the line wings) act as a pump in this region of the atmosphere, the increase in J_ν from C I and Si I opacities enhances this pump, further depleting the ground state and further enhancing the excited and ion states. This backflowing chromospheric ultraviolet radiation becomes very important in the ionization and excitation of neutral metals as will be demonstrated in Paper II. Table 8 lists various data concerning the ionization of the chromospheric-photospheric model of g Her.

We also test the effect helium has on the ionization and excitation of hydrogen by comparing runs where helium is handled in LTE (model D2) to NLTE (model D3) runs. The only effect seen is a slight decrease ($\sim 30\%$ maximum) in the collisional excitation rates for $10^{-7} < m < 10^{-6}$ g cm^{-2} (i.e., middle chromosphere) when helium is handled in NLTE due to the LTE assumption predicting an overionization in this region. At lower column masses (i.e., higher in the chromosphere), helium ionization nearly becomes complete and $b_\kappa \to 1$ while at higher column masses, neither hydrogen or helium are the dominant contributors to the electron density. The ionization of hydrogen is unchanged; however, the excited state densities drop by a few tens of percent in this region of the atmosphere. Essentially NLTE effects from helium have little impact on the excitation and ionization of hydrogen in this chromospheric model.

We next test the effect that partial redistribution (PRD) in the Lyα line has on the ionization and excitation of hydrogen in this model (model D4). We use the partial coherent scattering approximation of PRD as described by Avrett & Loeser (1984). Photon diffusion in the line wings are accounted for via the Hubený (1985) technique (see Luttermoser et al. 1989 for further details). PRD in the Lyα line has little effect on the

TABLE 8
IONIZATION OF HYDROGEN—g HERCULIS MODEL CHROMOSPHERE

Depth	m (g cm^{-2})	n_H (cm^{-3})	T_e (K)	$A_{21} \rho_{21}$ (s^{-1})	C_{21} (s^{-1})	τ_{21}[a]	n_κ/n_1[b]	n_κ/n_1[c]
1........	6.6(-15)	1.9(-3)	11270	5.5(4)	1.6(-11)	0.0	2.3(5)	4.4(8)
5........	2.6(-12)	0.82	10410	5.9(4)	6.6(-9)	6.0(-5)	5.3(2)	1.0(6)
10........	3.5(-6)	2.5(6)	8400	8.5(2)	6.4(-4)	9.1(4)	9.6(-3)	2.7
15........	2.1(-2)	2.6(10)	5300	59.	0.38	6.5(8)	4.9(-4)	3.6(-3)
20........	0.56	1.7(12)	2223	-18.	0.23	2.5(10)	8.2(-15)	7.3(-17)
25........	8.6	2.3(13)	2482	-0.34	1.9	3.9(11)	6.2(-15)	3.4(-15)
30........	1.6(2)	3.7(14)	2896	-0.39	31.	6.9(12)	3.9(-13)	3.3(-13)
35........	9.1(2)	1.8(15)	3398	-0.32	340.	7.8(13)	1.0(-10)	9.5(-11)
40........	1.6(3)	2.6(15)	4118	-0.56	2.1(3)	6.4(13)	7.1(-8)	6.9(-8)
45........	2.7(3)	3.1(15)	5688	-0.86	1.9(4)	1.0(14)	4.7(-4)	4.7(-4)

[a] Line center optical depth.
[b] Full statistical equilibrium calculations.
[c] Assumption of detailed balance in the Lyman lines.

ionization equilibrium in this model, except in the temperature minimum region (which supports our Lyα line wing/ionization analysis above), where there is a factor of 2 increase in the ion density just below the chromospheric temperature rise. At the same depths, the second level density is enhanced as well by a similar amount. The PRD approximation effectively *traps* photons in the line core to larger optical depths than the complete redistribution (CRD) approximation, which allows Lyα detailed balance to exist higher in the atmosphere. As a result, the excitation and ionization is controlled by the transfer in the line wings at this regime in the atmosphere. Photon diffusion in the wings acts to speed up the Lyα "pump," which results in an enhanced excitation and as a result, enhanced ionization. It is no surprise therefore that the only changes in the ionization and excitation occur in the temperature minimum region, where the line wing just outside the CRD core has an optical depth near unity.

The Lyman line DB approximation also effects the structure of the atmosphere. The DB overionization of hydrogen with respect to FSE causes an enhancement in the electron density in the upper layers of the chromosphere. Since the total number density increases at these layers and hydrostatic equilibrium is enforced in these models, the outer atmosphere expands by 30% under the assumption of Lyman-line detailed balance with respect to the model where all transitions are handled in detail.

3.2.2. *The TX Psc Model*

Figures 10a and 10b compare the number densities of the first three bound levels and the ion of hydrogen for the FSE calculations of the chromospheric-photospheric model (D2) and the pure photospheric model (A2) of TX Psc. Figures 11a and 11b are the corresponding plots of the departure coefficients. Although surface gravities and effective temperatures of g Her and TX Psc are similar, the radiation physics are very different in each. As demonstrated by Johnson, Luttermoser, & Faulkner (1988) in their comparison between an oxygen-rich and a carbon-rich models of 3000 K and log g = 0, carbon monoxide cooling in the outer layer extends deeper in the
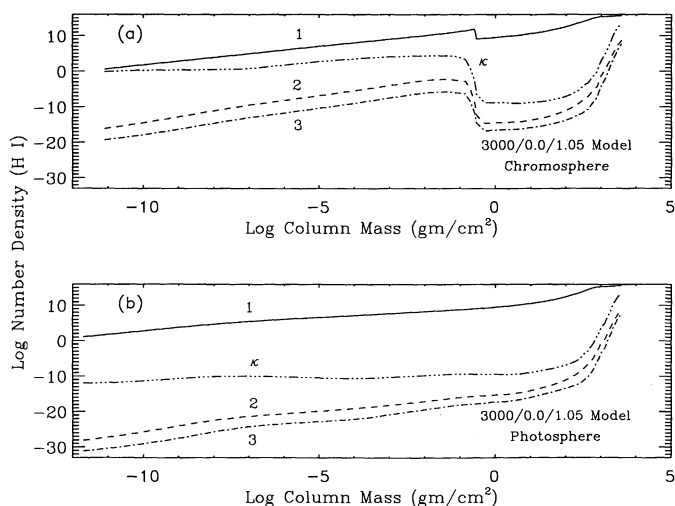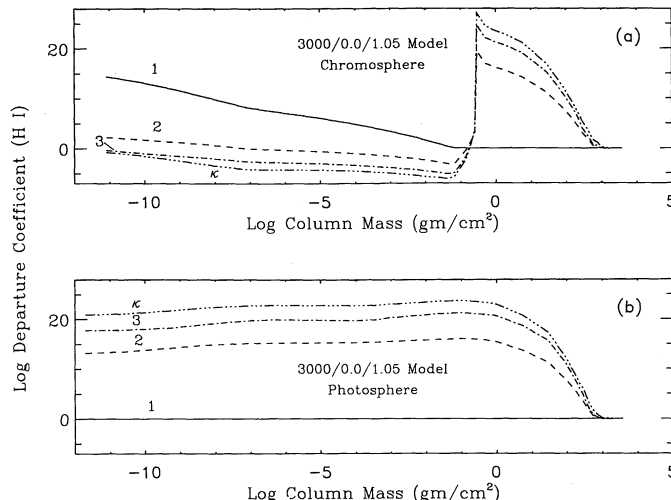
FIG. 11.—Effect of a chromosphere. The departure coefficients corresponding to the number densities of Fig. 10 for the atoms in the states $n = 1, 2, 3$, and κ (continuum = ion) for H I with full statistical equilibrium of the Lyman lines for either (a) a photosphere plus chromosphere or (b) a photosphere only, for the star TX Psc (C6,2).

carbon star model than the oxygen-rich model. This enhanced cooling increases the opacities of the neutral metals and molecules, which in turn lowers the pressures and densities in the outer layer. Hence, for a given Rosseland optical depth in these two models, the temperatures will be similar, but the densities will be much lower in the carbon star (or to look at it another way—for a given density, the middle and upper photosphere of a carbon star is cooler). The relatively higher density (as a function of optical depth) in the oxygen-rich star allows the Lyman lines to remain thermalized (i.e., $S_\nu = B_\nu$) at all photospheric depths except near the temperature minimum region due to the higher collisional rates (LJE). Another effect helps the Lyman lines to thermalize in the photosphere: additional cooling from the CO molecule drops the temperatures enough for molecular hydrogen to form throughout much of the photosphere. As a result, the Lyman lines and continuum are more transparent in the carbon-rich star than the oxygen-rich star. The higher optical depths in the M giant force $J_\nu = B_\nu$, hence LTE in the radiation field, higher in the atmosphere.

The Lyman line DB approximation has the same effect in this atmosphere as it has in the g Her (LJE) model: Hydrogen is *overionized* and *overexcited* chromospheric depths with the Lyman lines in detailed balance as compared to calculations where the lines are handled in detail; and is *underionized* and *underexcited* at photospheric depths. The DB approximation has a significant effect on the emergent spectrum. The overexcitation of hydrogen under this approximation is so great (a factor of 10^3–10^5 enhancement) that the Balmer lines become opaque in the chromosphere resulting in strong absorption features. Figure 12 displays a comparison between the Hα profile as calculated under the assumption of Lyman line detailed balance and as calculated with full statistical equilibrium. Since the Hα line is not seen among the CN lines near 6563 Å, observations further confirm that the DB approximation cannot be valid for the Lyman lines in cool, low-density environments. Recently, Mallik, Mallik, & Mohan Roa (1991) made similar observations for an NLTE analysis of G and K supergiants. (We take exception with one comment made in this paper: "The assumption of radiative detailed
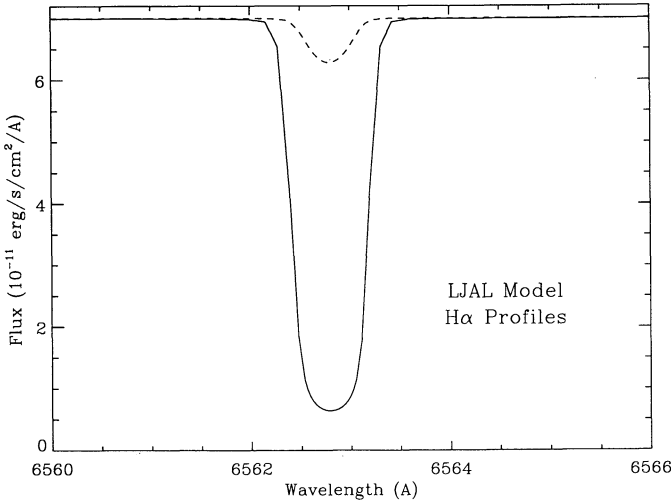
FIG. 10.——Effect of a chromosphere. Plotted are the number densities of the atoms in the states $n = 1, 2, 3$, and κ (continuum = ion) for H I with full statistical equilibrium of the Lyman lines for either (a) a photosphere plus chromosphere or (b) a photosphere only, for the star TX Psc (C6,2).

Fig. 12.—Profiles of the Balmer-α line in a combined photospheric-chromospheric model for TX Psc, for both detailed balance (*solid*) and full statistical equilibrium in the Lyman lines (*dashed*).

balance in the Lyman continuum and lines is certainly valid for the lower chromospheres of cool stars where the densities are high and the temperatures sufficiently low." We have shown here that *general* statements like this can lead to fundamental errors when applied to all cool giants, each star (or rather stellar type) is somewhat unique since the thermalization of the Lyman lines are sensitive to the atmospheric conditions.)

Hydrogen is strongly overionized in the upper and middle photosphere with respect to LTE. However, most of the hydrogen is in the ground state or in H_2, and hydrogen's contribution to the electron density is negligible at these depths. As such, this overionization has no effect on the emergent spectrum or the atmospheric structure.

As can be seen from Figures 11a and 11b, the attached chromosphere further overexcites and overionizes hydrogen in the upper photosphere to an even greater degree than the pure photosphere model, which we term *chromospheric back-warming* of these levels. This level pumping however is primarily due to the substantial increase of the ground-state photoionization rate and subsequent recombination to the excited states in the temperature minimum region in the chromospheric-photospheric model as compared to the identical region in the pure photospheric model. Comparing various rates between the two models show that the main difference is

the bound-free-bound rates ($\mathscr{P}$) for levels 1 to 2 and levels 1 to 3. At T_{min} in the chromospheric-photospheric model $\mathscr{P}_{12} = 5.5 \times 10^{-24}$ s^{-1} and $\mathscr{P}_{13} = 3.4 \times 10^{-24}$ s^{-1}, and at the corresponding depth (i.e., same temperature and density) in the photospheric model, $\mathscr{P}_{12} = 8.0 \times 10^{-28}$ s^{-1} and $\mathscr{P}_{13} = 5.0 \times 10^{-28}$ s^{-1}. The enhanced Lyman-continuum flux in the chromospheric-photospheric model and similar Lyman photo-recombination rates in the two models at the depths of interest leads to enhanced level populations of the excited states. Again it should be stressed that even though the excited levels are very overpopulated with respect to LTE, the number densities are small with respect to the ground and ionized states of hydrogen throughout the entire atmosphere. This is similar to the effect seen in the g Her model: however, it is more pronounced here and extends deeper into the photosphere. In this case, it is the Lyman continuum and *not* the Lyman lines that are responsible for the effect. In the upper photosphere of the TX Psc model, approximately 0.03%–0.1% of the total hydrogen density is in the neutral atomic state (i.e., nearly all hydrogen is in molecular form; note that the density jump seen in the ground state of hydrogen at log $m \sim -0.5$ g cm^{-2} in Figure 10a is due to the formation of molecular hydrogen), the Lyman continuum is transparent in these regions which allows the Lyman-continuum chromospheric photons to penetrate deep into the photosphere. The Lyman line wing transfer is unimportant at these depths due to the negligibly small opacity in the wings. Table 9 lists various data concerning the ionization of the chromospheric-photospheric model of TX Psc.

We also test the effect helium has on the ionization and excitation of hydrogen by comparing runs where helium is handled in LTE (model E2) to NLTE (model E3) runs. Like the g Her model, the only effect seen is a slight decrease ($\sim 10\%$ maximum) in the collisional excitation rates for $10^{-10} < m < 10^{-6}$ g cm^{-2} (i.e., upper/middle chromosphere) when helium is handled in NLTE due to the LTE assumption predicting an overionization, hence enhanced electron density, in this region. This portion of the LJAL model has similar temperatures ($T_e \sim 10^4$ K) to that of the LJE model where this effect was noticed. The ionization of hydrogen with respect to LTE is increased by a factor of 10 at these depths when helium is handled in NLTE. We wish to point out here that the LJAL model is not correct at depths where $T_e > 7000$ K ($m < 10^{-8}$ g cm^{-2}) since VLA measurements at 3.6 cm detected no signal from TX Psc—a 12.5 km s^{-1} wind radiating at 10^4 K would easily produce a detectable signal (Luttermoser & Brown 1992). Gas temperatures hotter than 7000 K do not exist in the

TABLE 9

IONIZATION OF HYDROGEN—TX PISCIUM MODEL CHROMOSPHERE

Depth	m (g cm^{-2})	n_H (cm^{-3})	T_e (K)	$A_{21}\rho_{21}$ (s^{-1})	C_{21} (s^{-1})	τ_{21}[a]	n_κ/n_1[b]	n_κ/n_1[c]
1.........	8.1(−12)	4.5	10000	2.5(4)	6.5(−9)	0.0	0.22	1.0(3)
5.........	4.2(−9)	3.3(3)	8300	6.9(3)	1.7(−6)	1.1(2)	8.6(−4)	2.1
10.........	5.5(−4)	6.0(8)	6050	8.3(2)	4.8(−3)	1.7(7)	1.5(−5)	1.6(−2)
15.........	6.7(−2)	9.4(10)	4700	1.7(2)	0.11	2.2(9)	2.1(−7)	4.3(−5)
20.........	0.29	2.8(12)	1239	−3.8	0.11	1.0(10)	3.1(−16)	2.9(−18)
25.........	28.	2.4(14)	1430	−2.3	2.8	1.1(10)	2.3(−20)	2.0(−21)
30.........	2.8(2)	1.6(15)	1980	−4.2	19.	2.0(11)	4.3(−19)	1.0(−20)
35.........	7.7(2)	2.5(15)	2550	−17.	51.	6.1(12)	5.4(−16)	9.8(−17)
40.........	2.0(3)	3.0(15)	4390	−1.1	1.7(3)	5.3(13)	5.8(−7)	5.5(−7)

[a] Line center optical depth.
[b] Full statistical equilibrium calculations.
[c] Assumption of detailed balance in the Lyman lines.

outer layers of TX Psc, which makes the helium NLTE effects on the hydrogen populations seen in this model atmosphere irrelevant in the *actual* stellar atmosphere.

We next test the effect partial redistribution (PRD) in Lyα has on the ionization and excitation of hydrogen (model E4). Hydrogen ionization remains virtually unchanged at all depths. The second and third level populations are reduced between 20% and 30% in the outermost layers in the PRD case and enhanced by a factor of 3 in the lower chromosphere. The temperature minimum region, however, displays no change. This effect is due to the Lyα wing radiative transfer. The Lyα "drain efficiency" is reduced due to the inability for core photons to scatter into the wings as they can under the CRD assumption. As such, the *core* stays in detailed balance which enhances the excited populations in the lower chromosphere. This effect is too small, however, to affect the Balmer line profiles, unlike the effect caused by the assumption of detailed balance for the *entire* line. Likewise, PRD effects reduce the source function in the outermost depths, which determines the n_2/n_1 ratio, hence reducing the excited level populations at those depths.

The Lyman line DB approximation again affects the structure of the atmosphere. The increased electron density (hence total particle density) in the outer layers, coupled with the hydrostatic equilibrium assumption, expands the atmosphere by 33% under the assumption of Lyman line detailed balance with respect to the model where all transitions are handled in detail. Comparisons between the CRD and PRD calculations show no change in the structure of the atmosphere in this or the g Her model.

4. HELIUM IONIZATION AND EXCITATION

The neutral helium calculations are carried out with a five-level model atom with three bound-bound transitions. Photoionizations and recombinations are included for all bound levels. He II calculations are not made since the He I ionization is entirely negligible in the photospheric models and throughout most of the atmospheric depths of the chromospheric-photospheric models. The excited states of He I all lie at high energies (lowest lies near ~20 eV) and are virtually unpopulated in the photospheric models and throughout the lower layers of the chromospheric-photospheric models. These states and transitions between the states have no impact whatsoever on the emergent spectrum or structure of the pure photospheric models. Minor changes are noted for the atmospheric structure of the upper chromospheres.

4.1. *Photospheric Models*

Figure 13 shows the number densities of the five bound levels and ion in the photospheric model of g Her (model A3). Similar results are found for the two carbon star photospheric models. In a sense, the ionization and excitation of helium in the photosphere, is almost trivial, for there is vanishingly little of either. For this reason, we discuss both the M giant and the carbon star photospheres together.

As expected, in either LTE or NLTE, helium is neutral by an enormous factor throughout these photospheric models (A3, B3, and C3). Departure coefficients for the ion and bound states are very similar in both shape and magnitude to those of hydrogen for the respective models. This is no accident since, like the hydrogen atom, the ion and excited states densities are controlled by bound-free-bound rates out of the ground state. The resonance transition at $\lambda584$ ($5 \to 1$) is far from being in

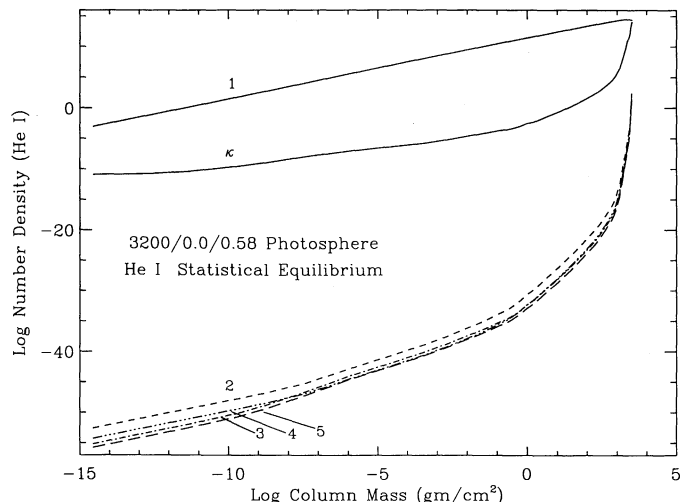FIG. 13.—Ionization and excitation for He I. Plotted are the number densities of the atoms in the states $n = 1, 2, 3, 4, 5$, and κ (continuum = ion) for He I for a photospheric model for the star g Her (M6 III). Please see text for a description of the atomic model.

detailed balance, since the net radiative rate $A_{51}\rho_{51}$ is comparable to the bound-free-bound rate $\mathscr{P}_{51}$ throughout the entire atmosphere (the collisional rate C_{51} is negligible throughout much of these atmospheres, reaching a maximum strength, relative to $A_{51}\rho_{51}$, of 2%–7% deep in the atmosphere ($m > 10^3$ g cm^{-2}) of the various models. As a result, helium population densities only reach equilibrium values at only the deepest layers of these models. Once again, the UV resonance line acts as a "pump" for the excited levels. The extreme weakness of the far ultraviolet radiative flux makes this a much less efficient pump than the Lyα line. Once an electron has been excited to the $2p \, ^1P^o$ level via the $\lambda584$ transition, ionization occurs rapidly from the photospheric radiation field at $\lambda3681$.

Finally, due to the extremely low ion densities of helium in these models, NLTE effects have no impact on either the emergent spectrum or atmospheric structure of these models. The ground-state density is a large reservoir and as such $b_1 = 1$ at all depths; hence the resonance line opacity remains equal to the LTE opacity values (neglecting PRD effects). The excited states have such low densities that no transition out of these states will be seen. The low-ionization state of helium dictates that helium plays no role as a source of electrons and hence does not affect the structure of the atmosphere in any way. As a result, NLTE effects in helium do not alter the population densities and radiative rates in the hydrogen calculations.

4.2. *Photospheric plus Chromospheric Models*

As was seen in the previous section, helium can be handled in LTE in modeling cool stellar photospheres due to the negligible effect NLTE radiative transfer has on the emergent spectrum and electron populations. We must now ask whether the chromospheric temperature rise influences the atmospheric structure and/or emergent spectrum.

4.2.1. *The g Her Model*

Figure 14 shows the number densities as a function of column mass of the five bound levels and ion of our neutral helium atom for the g Her chromospheric-photospheric model. As can be seen, helium becomes mostly ionized in the upper chromosphere ($m > 10^{-8}$ g cm^{-2}) of this model. Excited state
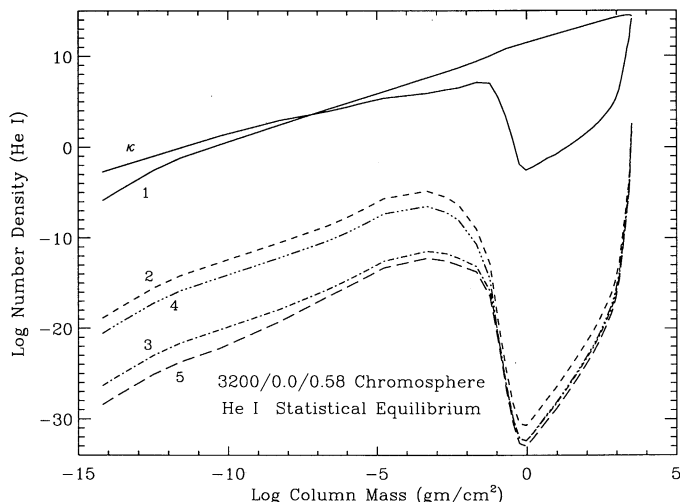
FIG. 14.—Number densities of the atoms in the states $n = 1, 2, 3, 4, 5$, and κ (continuum = ion) for He I for a model photosphere plus chromosphere for the star g Her (M6 III).

populations are also enhanced in the chromosphere in comparison to similar column masses in the pure photospheric model, although not enough to produce any observables features from these levels. Figures 15a and 15b show a comparison of the departure coefficients for the chromosphere-photosphere (D3) and pure photosphere (A3) models. As is the case for hydrogen, chromospheric backwarming affects the ionization and excitation equilibria in the upper photosphere. Another interesting feature is the fact that helium is under-ionized in the chromosphere with respect to LTE, an effect that has already been noted in the hydrogen section of the paper. Since the source functions are partially coupled to the photospheric radiation field ($J_v \ll B_v$) in the NLTE case instead of being directly coupled to B_v, underionization with respect to LTE results. In the regime around 8000 K, hydrogen is nearly (but *not* fully) ionized, which allows the NLTE effects in the hel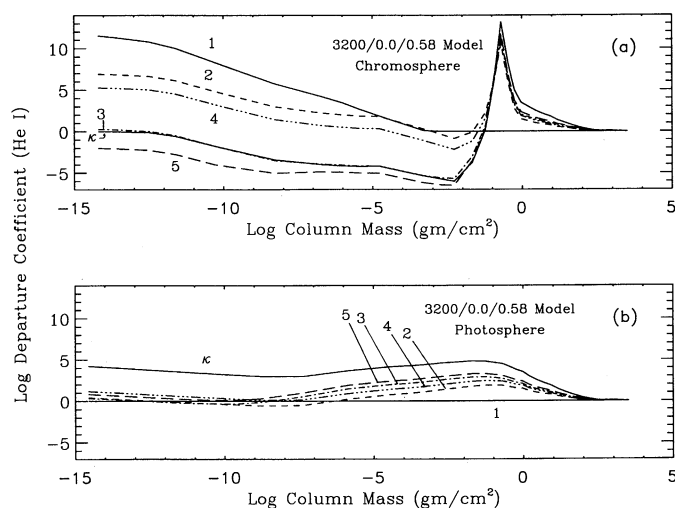ium ionization to alter the electron density. At hotter temperatures, b_κ approaches unity due to helium becoming fully ionized and helium's contribution to the electron population approaches that of LTE. For cooler temperatures, helium is almost fully neutral and plays no role in the electron population. This underionization of helium with respect to LTE in the upper chromosphere causes a small decrease in the electron density, which in turn, contracts the atmosphere by 4% in a hydrostatic equilibrium atmosphere.

4.2.2. *The TX Psc Model*

Figure 16 displays the level densities of levels 1, 2, 3, 4, 5, and κ for the He I atomic model used in the E3 atmospheric model of TX Psc. Like the g Her chromosphere, the ionization and excitation is enhanced in the chromosphere with respect to corresponding depths in the pure photosphere model. Unlike the g Her model, the temperature of the TX Psc model never exceeds 10^4 K and He I stays neutral at all depths in the atmosphere except for the very uppermost layers of the chromosphere. Recall that it was at these depths where helium's contribution to the electron density became significant and had some impact on the ionization and excitation equilibria of hydrogen. Once again, however, the enhanced number densities of the excited states in the chromosphere of this model have no effect on spectral features associated with these levels.

Once again the ionization of helium is lower in the NLTE case as compared to the LTE case at chromospheric depths. The lower electron density that results from this leads to a decrease in the size of the chromosphere by 3%—a negligible amount with respect to the uncertainties in the temperature-density stratification in this region of the atmosphere.

In summary, the ionization and excitation of helium has no effect on the emergent spectrum (except for the ground-state bound-free edge and resonance line, which will have to wait for much more sensitive telescopes before being detected) and has a small effect on the electron density at chromospheric depths when $T_e > 8000$ K. The atmospheric structure is slightly altered but negligible with respect to the observational uncertainties of this semiempirical atmosphere.
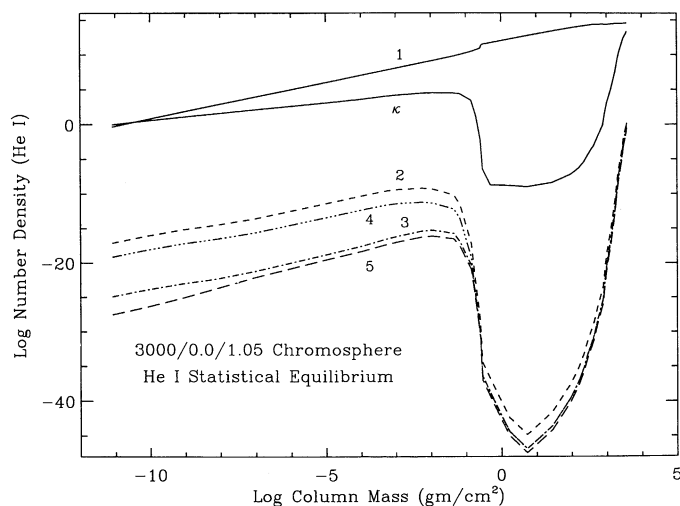

FIG. 15.—Effect of a chromosphere. The departure coefficients for the atoms in the states $n = 1, 2, 3, 4, 5$, and κ (continuum = ion) for He I for either (a) a photosphere plus chromosphere or (b) a photosphere only, for the star g Her (M6 III).

FIG. 16.—Number densities of the atoms in the states $n = 1, 2, 3, 4, 5$, and κ (continuum = ion) for He I for a model photosphere plus chromosphere for the star TX Psc (C6,2).

5. DISCUSSIONS AND CONCLUSIONS

Before presenting conclusions of this work, we comment on the various difficulties in NLTE radiative transfer of "ultracool" stellar atmospheric models. The first difficulty to note is the extreme low densities that are required in the outer layers to allow the Lyman lines and continuum to become optically thin, which is needed to solve the transfer equation for these transitions. Typically for coronal stars, hydrogen ionizes quickly in the transition region forcing the Lyman transitions to low-opacities. However, in these cool, noncoronal stars, the only way to reduce the Lyman opacities is to extend the atmosphere to interstellar medium densities *or* to hope that sufficient quantities of molecular hydrogen form. Although the temperatures are cool enough in the pure photospheric models, molecular hydrogen formation is a three-body process which requires a sufficiently high density for the molecule to form. When one gets to column masses less than 10 g cm^{-2} in the g Her model and 1 g cm^{-2} for the diatomic TX Psc model, the molecular hydrogen–to–total hydrogen density ratio begins to decrease as a result of the decrease in density, even though the temperatures continue to drop. As has been shown by Bowen (1988), however, hydrodynamic processes in late-type pulsators pump up the density in the outer layers which may help in the molecular formation process; unfortunately, the radiation field from the emerging shocks tends to dissociate hydrogen readily in the outer layers (Luttermoser & Bowen 1992). We earlier noted that our "pure" photospheric models are radiative equilibrium models. This is true only out to column masses of $\sim 10^{-5}$ g cm^{-2} since modelers tend not to go to lower densities due to the difficulty in the radiative equilibrium temperature correction (i.e., Avrett-Krook technique) convergence in these regimes. The outer layers of our "extended" photospheric models are just a temperature/density extrapolation from the outermost layers of the radiative equilibrium models.

Another difficulty that arises in these low-density environments is the large number of iterations required to converge a model. In our equivalent two-level approach, upward of 200 iterations may be typically required to converge the three-level hydrogen atom in the pure photospheric environments if one is not careful in solving the statistical equilibrium equations. Avrett & Loeser (1987) discuss this problem in detail for the three-level hydrogen atom, and we summarize it here. In optically thick regions where $\rho \ll 1$, ρ should be calculated via

$$\rho_{ji} = \epsilon_{ji}\left(\frac{\mathscr{B}_{ji}}{S_{ji}} - 1\right), \qquad (20)$$

where ϵ and $\mathscr{B}$ for the 21 transition depend on ρ for the 31 and 32 transitions, and ϵ and $\mathscr{B}$ for the 32 transitions depend on ρ for the 21 and 31 transitions, etc., whereas in optically thin regions, ρ is not necessarily small compared to unity, and it is more appropriate to use equation (12). Avrett & Loeser then use a linear combination of equations (12) and (20) at small optical depths:

$$\rho_{ji} = (1 - w_{ji})\rho_{ji}^o + w_{ji}\rho_{ji}', \qquad (21)$$

where ρ_{ji}^o is given by equation (20), ρ_{ji}' is given by equation (12), and where w_{ji} typically has the value 0.5 in the region of the atmosphere where τ_{ji} for the strongest line is no greater than about 10. This specific prescription does not work in these ultra–low-density environments however. When collisional rates are very low, we find quicker convergence by letting $w_{ji} \approx 0.99$–0.999 for $\tau_{ji} < 10$ *specifically* for each line and *not* in

reference to the strongest line. In these cool, low density environments, $\bar{J}_{ji} > S_{ji}$ due to the extremely low values of the Planck function, which results in a negative net radiative rate (i.e., more absorptions than emissions). If these rates become too negative, they easily outweigh the photoionization and collisional rates, which in turn give rise to negative source functions and departure coefficients. Even with the above recipe, convergence typically required 50–100 iterations. Note that convergence is achieved somewhat faster in the chromospheric-photospheric models. Also note that no problems were experienced with the helium calculations, even in the pure photosphere cases, where convergence is achieved in typically 10 iterations.

We have studied the ionization and excitation equilibria through detailed radiative transfer calculations for very cool ($T_{eff} < 3500$ K) giant and supergiant stars for the first time. NLTE effects in pure photospheric models and semiempirical chromospheric models are investigated. The results found in this study differ quantitatively from Auman & Woodrow (1975). Their assumption of detailed balance in all bound-bound transitions led directly to the result that densities of excited state densities are determined solely by the ionization equilibrium from these levels, which overestimates these densities at chromospheric temperatures and underestimates these densities in photospheric regimes.

The results ascertained in this study are summarized as follows:

1. Non–LTE effects are substantial in late-type giant and supergiant stellar atmospheres which lead to enhanced number densities in excited bound states in the middle and upper photosphere (T_{min} region in chromospheric-photospheric models) due to the source function coupling to the photospheric mean intensity instead of the Planck function.

2. Although hydrogen is extremely overexcited and overionized with respect to LTE at photospheric depths, hydrogen is primarily neutral or in molecular form in these cool models.

3. NLTE effects in hydrogen are negligible in the emergent spectrum for all models (pure photosphere and chromosphere-photosphere) and has no impact on the electron densities for all models, except for the extreme uppermost layers of the chromospheric models.

4. The assumption of detailed balance for optically thick lines in low-density atmospheres is not valid and tends to overestimate/underestimate level populations and ionizations at chromospheric/photospheric depths, since the Lyman lines are not allowed to *drain/pump* the excited levels.

5. Number densities for excited and ionized states in the middle and upper photosphere can be enhanced above photospheric NLTE effects through *chromospheric backwarming*, where chromospheric photons shine back onto the photosphere, increasing J_ν at those depths.

6. Radiative equilibrium atmospheres converged with polyatomic molecular opacities have hydrogen ionization and excitation equilibria that are fundamentally different than models converged with diatomic opacities alone.

7. The Lyman lines (especially Lyα) control the ionization and excitation of hydrogen in these models, except for the upper photosphere of the TX Psc chromospheric-photospheric model, where the Lyman continuum dominates the transfer.

8. Carbon abundance influences the ionization and excitation of hydrogen through the strong C I bound-free opacity under the Lyman lines—carbon stars are overionized and overexcited in hydrogen as compared to oxygen-rich stars of similar effective temperature and surface gravity.

9. PRD effects in Lyα have significant consequences in the ionization and excitation of hydrogen in the T_{min} region of the g Her chromospheric-photospheric model and the chromosphere of the TX Psc model.

10. NLTE He I ionization and excitation equilibria have a small effect on the electron density in the upper chromospheres of these models and have no effect on the emergent flux of these models and essentially no effect on the structure of the atmospheres.

Paper II will discuss the results of detailed radiative transfer in the ionization and excitation in the neutral metals C, Na, Mg, and Ca. These metals are of fundamental importance since they are the major contributor to the electron density, hence H^- opacity, throughout most of the photosphere and lower chromosphere. As well, the ionization and excitation of these metals have a substantial impact on the emergent spectrum of these stars, particularly in the ultraviolet.

REFERENCES

Aggarwal, K. M., Kingston, A. E., & McDowell, M. R. C. 1984, ApJ, 278, 874
Auman, J. R., & Woodrow, J. E. J. 1975, ApJ, 197, 163
Avrett, E. H. 1968, in Resonance Lines in Astrophysics, ed. R. G. Athay, J. Mathis, & A. Skumanich (Boulder: NCAR), 27
Avrett, E. H., & Loeser, R. 1984, in Methods in Radiative Transfer, ed. W. Kalkofen (Cambridge: Cambridge University Press), 341
———. 1987, in Numerical Radiative Transfer, ed. W. Kalkofen (Cambridge: Cambridge Univ. Press), 135
Avrett, E. H., Vernazza, J. E., & Linsky, J. L. 1976, ApJ, 207, L199
Bowen, G. H. 1988, ApJ, 329, 299
Brown, J. A., Johnson, H. R., Alexander, D. R., Cutright, L., & Sharp, C. M. 1989, ApJS, 71, 623
Carbon, D. F. 1979, ARA&A, 17, 513
Chang, E. S., Avrett, E. H., & Loeser, R. 1991, A&A, 247, 588
Desikachary, K., & Gray, D. F. 1978, ApJ, 224, 1073
Dimitrijevic, M. S., & Sahal-Bréchot, S. 1984, J. Quant. Spectros. Rad. Transf., 31, 301
Eaton, J. A., & Johnson, H. R. 1988, ApJ, 325, 355
Hartmann, L., & Avrett, E. H. 1984, ApJ, 284, 238
Hubený, I. 1985, A&A, 145, 461
Johnson, H. R. 1982, ApJ, 260, 254
———. 1986, in The M-Type Stars, ed. H. R. Johnson & F. Querci (NASA SP-492), 323
———. 1991, A&A, 244, 462
Johnson, H. R., Jørgensen, U. G., & Luttermoser, D. G. 1991, in Mechanisms of Chromospheric and Coronal Heating, ed. P. Ulmschneider, E. R. Priest, & R. Rosner (Heidelberg: Springer), 200
Johnson, H. R., & Luttermoser, D. G. 1987, ApJ, 314, 329

Johnson, H. R., Luttermoser, D. G., & Faulkner, D. R. 1988, ApJ, 332, 421
Jordan, C. 1986, in New Insights into Astronomy: 8 Years of UV Observations with IUE, ed. E. Rolfe (ESA SP-263), 17
Jørgensen, U. G. 1989, ApJ, 344, 901
Jørgensen, U. G., Almlöf, J., Gustafsson, B., Larsson, M., & Siegbahn, P. 1985, J. Chem. Phys., 83, 3034
Jørgensen, U. G., & Johnson, H. R. 1991, A&A, 244, 462
Judge, P. G. 1986a, MNRAS, 221, 119
———. 1986b, MNRAS, 223, 239
———. 1989, in Evolution of Peculiar Red Giant Stars, ed. H. R. Johnson & B. Zuckerman (Cambridge: Cambridge Univ. Press), 303
Kono, A., & Hattori, S. 1984, Phys. Rev. A, 29, 2981
Luck, R. E., & Lambert, D. L. 1982, ApJ, 256, 189
Luttermoser, D. G. 1992, in preparation (Paper II)
Luttermoser, D. G., & Bowen, G. H. 1992, in preparation
Luttermoser, D. G., & Brown, A. 1992, ApJ, 384, 634
Luttermoser, D. G., Johnson, H. R., Avrett, E. H., & Loeser, R. 1989, ApJ, 345, 543 (LJAL)
Luttermoser, D. G., Johnson, H. R., & Eaton, J. A. 1992, in preparation (LJE)
Mallik, S. V., Mallik, D. C. V., & Mohan Roa, D. 1991, A&A, 243, 463
Mathisen, R. 1984, Inst. Theor. Astrophys. Publ., Olso Univ., No. 1
Mendoza, E. E. 1983, in IAU Symp. 103, Planetary Nebulae, ed. D. R. Flower (Dordrecht: Reidel), 143
Ramsey, L. W. 1977, ApJ, 215, 827
Vernazza, J. E., Avrett, E. H., & Loeser, R. 1973, ApJ, 184, 605 (VAL I)
———. 1976, ApJS, 30, 1 (VAL II)
———. 1981, ApJS, 45, 635 (VAL III)